ARTICLE

Synthesis of ZnS loaded biochar nanocomposite and application towards Pb^{2+} ions removal: An RSM based optimization

V. Vandhana Devi[1], S. Radjarejesri[2], Pandurangan Selvaganapathi[3] and R. Lakshmipathy[4,*]

[1] Department of Education, National Institute of Technical Teachers Training and Research, Chennai, India
[2] Department of Science, Sona College of Technology, Salem-636005, Tamilnadu, India
[3] Department of Chemistry, SRM TRP Engineering College, Tirchy-621105, Tamilnadu, India
[4] Directorate of Learning and Development, SRM Institute of Science and Technology, Kattankulathur, Tamilnadu, India-603203

Abstract

The present study reports the synthesis of ZnS nanoparticles via green synthesis route and loading them onto the jamun seeds biochar to prepare a nanocomposite. The synthesized nanocomposite were characterized with FTIR, XRD and SEM. The synthesized ZnS nanoparticles were found to be spherical in shape with size less than 5 nm. SEM images confirmed the loading of ZnS nanoparticles onto the biochar. The nanocomposite was employed in the removal of Pb^{2+} ions using a developed CCD by RSM. The significance of the model was supported by the p-value being less than 0.0001 and higher F-value. The loading capacity of the ZnS loaded biochar is calculated to be 211.0 mg g^{-1}. The isotherm and kinetic investigations suggest the applicability of Langmuir and Pseudo second order models to the equilibrium data. The spontaneity of the process is well supported by the thermodynamic values. 0.1 M HCl exhibited highest desorption ability compared to other desorbing agents and successfully regenerated the nanocomposite. The ability of the ZnS loaded biochar nanocomposite to successfully eliminate the Pb^{2+} ions was demonstrated and unveils the real time applications in waste water treatments.

Keywords: ZnS, Biochar, Lead, Nanomaterials

Citation
V. Vandhana Devi, S. Radjarejesri, Pandurangan Selvaganapathi and R. Lakshmipathy (2026). Synthesis of ZnS loaded biochar nanocomposite and application towards Pb^{2+} ions removal: An RSM based optimization. Mari Papel Y Corrugado, 2026(1), 25–33.

1 Introduction

Heavy metal ions are proven to be serious environmental contaminants and presence of heavy metal ions in aqueous streams has significant impact on aquatic life [1]. Increasing population and demand for finished products has resulted in release of heavy metal ions in aqueous streams. Due to versatile applications, Lead is used in several industries such as battery, paint, chemical, automotive and construction etc., and are easily released into water streams [2]. Presence of lead ions (Pb^{2+}) in aqueous streams effects aquatic life and human health due to their carcinogenicity [3]. Hence it is essential to eliminate Pb^{2+} ions from effluents before they are released into the water streams. Various treatment techniques are in practice for the removal of Pb^{2+} ions from aqueous solutions however, adsorption is considered to be unique and most beneficial technique due to ease of process and economic feasibility [4].

Submitted: 17 November, 2025
Accepted: 15 January, 2026
Published: 28 January, 2026

Vol. 2026, **No.** 1, 2026.
https://doi.org/10.71442/mari2026-0003

***Corresponding author:**
✉ R. Lakshmipathy
lakshmipathy.vit@gmail.com

Materials starting from activated carbon to agriculture waste are explored as adsorbents for removing Pb^{2+} ions [5]. Agriculture wastes and by-products are explored as potential adsorbents due to their abundance and low cost. Agrowastes such as banana peels, orange peels [6], watermelon rinds and custard apple shells [7] were potentially explored as adsorbents. Surface modification of the agrowastes has enhanced their efficiency towards Pb^{2+} ions removal from aqueous solutions. A surface modification with acids and bases and conversions into biochars has increased the removal efficiency. Further additions of nanomaterials onto the biochars amplify the removal process with multifold increase in the loading capacities. In a study by Iqbal et al [8], hematite-loaded *Saccharum munja* biochar was evaluated to remove Cd^{2+} ions from aqueous solution. The results showed 20 % increase in loading capacity compared to biochar without nanomaterial loading. In another study, ZnO nanomaterials were loaded onto rice husk biochar and evaluated for the removal efficiency towards reactive red 24 from aqueous solution [9]. Removal of Pb^{2+} ions was explored using Meghemite functionalized with EDTA loaded biochar from aqueous solution [10]. The results revealed higher adsorption capacity compared to various adsorbents. A useful review on the nanomaterials loaded biochar was reported which provides deeper insights into the nano-biochar composites [11].

Considering the potential advantages of the nanomaterial loaded biochars, this study aims at the preparation of jamun seeds based biochar and jamun seed extract based synthesis of ZnS nanoparticles and further preparation of ZnS nanoparticles loaded biochar. The prepared nanocomposite will be explored for the removal of Pb^{2+} ions from aqueous solutions in batch process.

2 Materials and methods

2.1 Preparation of extract

The jamun seeds were powdered using a conventional mixture and the mixture was sieved using a mesh to obtain a uniform particle size. To 100 ml of distilled water, 0.10 g of seed powder was mixed and heated on magnetic stirrer with constant stirring for 60 min. Later the mixture was filtered to obtain the seed extract and the extract was used for the synthesis of ZnS nanoparticles. The solid material obtained after biomolecule extract was dried in oven for further use.

2.2 Preparation of biochar

The oven dried jamun seeds after extraction was mixed with NaOH in 1:1 ratio and placed in an oven at 90 °C for 120 min. After heating for fixed time, the jamun seeds were converted to biochar and the biochar was washed repeatedly in order to remove the excess NaOH and neutralize the pH of the biochar. After wash, the biochar was dried in an oven and stored in air tight containers for further use.

2.3 Synthesis of ZnS nanoparticles

Preparation of ZnS nanoparticles were performed as reported in literature [12]. 0.1M Zinc acetate solution was prepared freshly and to 50 ml of 0.1M Zinc solution, 20 ml of freshly prepared jamun seeds extract was added with constant stirring. To the mixture, 0.1 M Na_2S solution of 50 ml was added drop by drop with constant stirring and formation of white precipitate was observed on addition of the sulphide source. The mixture was stirred further for 60 mins in order to make sure all the Zn ions react with S^{2-} ions to form ZnS nanoparticles. The suspension was centrifuged and the pellet was dried in oven to obtain the ZnS nanopowder.

2.4 Preparation of ZnS nanoparticles loaded biochar

Firstly, 0.5 g of ZnS nanoparticles were added to distilled water with constant stirring to obtain nano suspension. Then the dried biochar 0.5 g was added to 50 ml of distilled water to prepare a suspension. To the biochar suspension, freshly prepared nano suspension was added drop by drop with constant stirring and after addition of all nano suspension the stirring was continued further for 60 min. the stirring helped in addition of the ZnS nanoparticles on the surface of the biochar. After stirring the mixture was filtered and the solid product was dried in oven and used for further characterization.

2.5 Batch adsorption experiments

The adsorption of Pb^{2+} ions onto ZnS-loaded biochar was studied through batch adsorption experiments, where key independent variables were systematically varied. The optimization of these variables was conducted using the Central

Composite Design (CCD) approach within Response Surface Methodology (RSM). Each experiment utilized 50 mL of test solution and was carried out in an orbital shaker set to 100 rpm. A full factorial design comprising 20 experiments was implemented to efficiently fit data and develop predictive models. The critical factors and their corresponding details are summarized in Table 1. The CCD setup and model construction were performed using Design Expert 13 software. The residual concentration and removal percentage were calculated using the following equations

$$\%\ Pb^{2+}\ ion\ adsorption = \frac{C_0 - C_1}{C_0} x100 \quad (1)$$

$$Adsorption\ capacity = \frac{C_0 - C_1}{m} xV \quad (2)$$

3 Results and discussion

3.1 Characterization of ZnS loaded jamun seed biochar

Identification of functional groups on the surface of the ZnS loaded biochar was performed using FTIR analysis and the spectra is represented in Fig. 1. The spectra displayed a number of peaks indicating the presence of variety of functional groups. A broad peak at 3479 cm^{-1} confirms the presence of –OH group and it asymmetrical peak is observed at 1629 cm^{-1}. Peaks at 1402, 1192 and 1111 cm^{-1} corresponds to C-O symmetric stretching of carbooxylates and ethers [13]. A weak peak at 445 cm^{-1} is due to Zn-S bond vibrations confirming the presence of ZnS nanoparticles on the surface on the biochar [12].

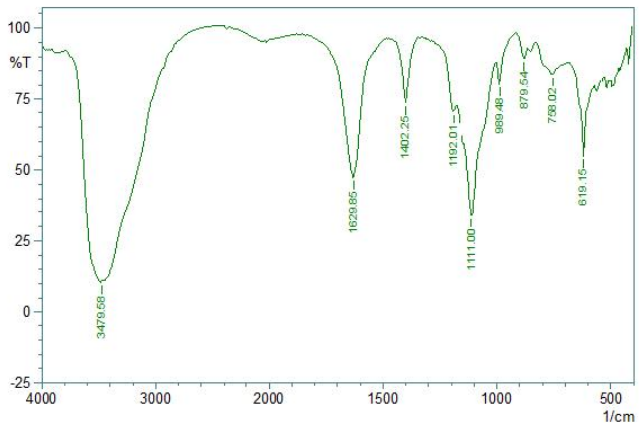

Figure 1. FTIR of ZnS loaded jamun seed biochar nanocomposite

X-ray diffraction (XRD) analysis was conducted to determine the crystalline structure of ZnS nanoparticles synthesized using Jamun seed extract loaded biomass (Fig.2). Diffraction peaks observed at 28.65°, 47.56°, 56.44°, were indexed to the (111), (220) and (311) planes of cubic ZnS, respectively [14]. The diffraction peaks exhibited noticeable broadening, indicating the nanoparticles' small size. This broadening is characteristic of the size effect associated with nanoscale particles. The calculated lattice parameters align well with the standard values provided in JCPDS No: 03-065-0309, and no impurity-related peaks were detected. A broad peak around 21.37° indexed to (002) plane confirms the presence of disordered aromatic structures of biochar. These evidences confirm the successful integration of ZnS nanoparticles onto the jamun seeds biochar.

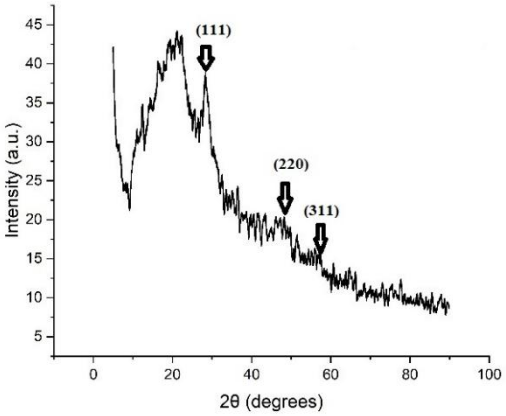

Figure 2. XRD pattern of ZnS-loaded biomass

Transmission Electron Microscope analysis was performed to understand and confirm the formation of ZnS nanoparticles (Fig. 3). The sizes of ZnS nanoparticles were found to be spherical in shape with size less than 5 nm. The small sizes observed in the images are well supported by the XRD peak broadening observed earlier.

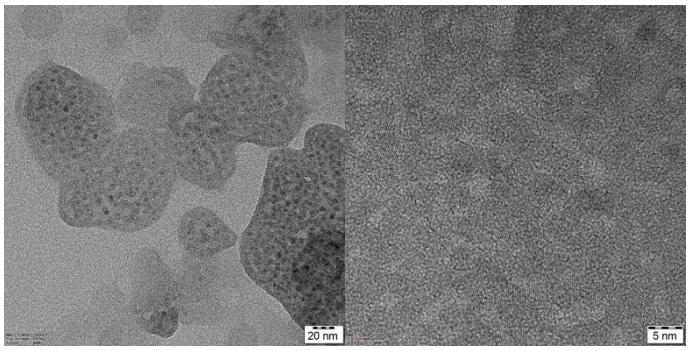

Figure 3. TEM image of ZnS nanoparticles synthesised using jamun seed extract

Scanning electron microscopy analysis was performed for the ZnS nanoparticles loaded biochar (Fig.4). The surface of the biochar are not regular

and appears to be porous and interestingly ZnS nanoparticles loaded on the surface are spotted as clusters as shown with the arrow marks in Fig. 4. It is also noticed the presence of some sharp needle like structure of the biochars and this might be the fibres of the seeds.

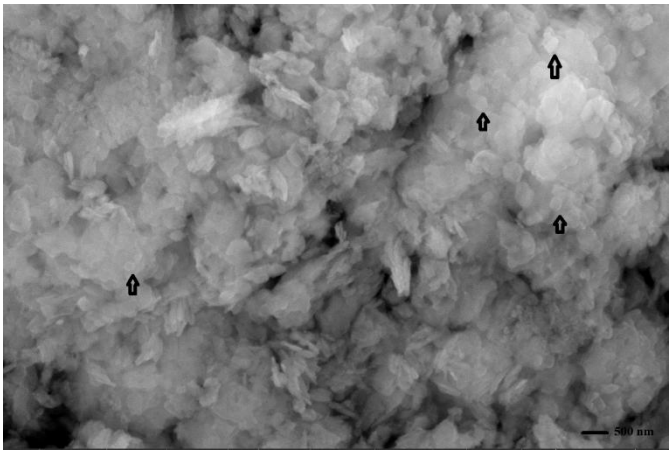

Figure 4. SEM image of ZnS nanoparticle loaded jamun seeds biochar

3.2 RSM investigations

A central composite design (CCD) was employed to optimize Pb^{2+} ion adsorption using ZnS-loaded biochar, focusing on three variables: pH, contact time, and initial Pb^{2+} concentration. The CCD comprised 20 runs, including 6 axial points, 6 central points, and 8 cubic points. Tables 1 and 2 summarize the experimental and predicted design matrices and ANOVA results for Pb^{2+} removal. A quadratic model, developed using Design Expert 13, produced a second-order polynomial equation (Equation 3) to describe the relationship between the variables and Pb^{2+} removal efficiency.

$$\%\text{Removal} = 91.58 + 2.06A + 8.40B - 7.88C - 24.33A^2 - 12.83B^2 - 3.76C^2 - 1.79AB - 12.83AC + 6.11BC \quad (3)$$

The quadratic equation (Equation 3) highlights the influence of pH, contact time, and initial Pb^{2+} concentration on the adsorption efficiency of ZnS-loaded biochar. Positive coefficients suggest that higher levels of a factor enhance adsorption, while negative coefficients indicate reduced efficiency. The equation also incorporates two-factor interaction and curvature terms, reflecting the combined and nonlinear effects on adsorption. A strong correlation between predicted and experimental results (Table 1) validates the model, confirming its reliability and the enhanced adsorption observed in the experiments.

Table 1. Runs of CCD with comparison of experimental and theoretical % removal for the removal of Pb^{2+} ions by ZnS loaded biochar

		Factor 1	Factor 2	Factor 3	Removal %	
Std	Run	A:pH	B:Contact time (min)	C:Initial concentration (mg/L)	Experimental	Predicted
19	1	6	75	100	90.5	91.58
2	2	8	30	50	60.2	61.47
3	3	4	120	50	56.4	59.20
15	4	6	75	100	90.6	91.58
1	5	4	30	50	47.6	51.04
17	6	6	75	100	90.7	91.58
13	7	6	75	15	98.4	94.12
6	8	8	30	150	27.3	30.76
11	9	6	10	100	56.2	52.68
9	10	3	75	100	39.5	33.74
7	11	4	120	150	53.4	58.38
8	12	8	120	150	53.4	56.21
10	13	9	75	100	45.3	39.94
16	14	6	75	100	90.7	91.58
12	15	6	150	100	76.3	69.94
14	16	6	75	180	74.3	69.35
20	17	6	75	100	91	91.58
18	18	6	75	100	90.8	91.58
5	19	4	30	150	24.2	25.78
4	20	8	120	50	57.8	62.47

Table 2. ANOVA for the removal of Pb^{2+} ions by ZnS loaded biochar

Source	Sum of Squares	df	Mean Square	F-value	p-value
Model	9957.30	9	1106.37	143.83	< 0.0001
A-pH	53.25	1	53.25	2.11	0.1770
B-Contact time	894.61	1	894.61	35.44	0.0001
C-Initial concentration	833.00	1	833.00	33.00	0.0002
AB	25.56	1	25.56	1.01	0.3380
AC	14.85	1	14.85	0.5883	0.4608
BC	298.90	1	298.90	11.84	0.0063
A^2	6096.49	1	6096.49	241.50	< 0.0001
B^2	1909.59	1	1909.59	75.64	< 0.0001
C^2	194.35	1	194.35	7.70	0.0196
Residual	252.45	10	25.24		
Lack of Fit	252.30	5	50.46	17.88	< 0.1029
Pure Error	0.1483	5	0.0297		
Cor Total	10209.74	19			
R^2	0.9753		Predicted R^2	0.8123	
Adjusted R^2	0.9530		Adeq Precision	19.2369	

The ANOVA results presented in Table 2 validate the effectiveness of the model in predicting Pb^{2+} removal using ZnS-loaded biochar. The extremely low p-value (<0.0001) indicates the model's

statistical significance, showing that the findings are highly unlikely to result from random variation. A high F-value of 43.83 further supports the model's reliability, reflecting a very low probability (0.01%) of the results occurring by chance. Additionally, a lack of fit F-value greater than 0.1 suggests that the unexplained variation within the model is minimal. Figure 5d demonstrates the alignment between predicted and actual values, with data points evenly distributed along a straight line, confirming normal data distribution without significant anomalies, thus removing the need for data transformation. The model's accuracy is further evidenced by a correlation coefficient of 0.975, along with high adjusted and predicted R-squared values of 0.953 and 0.953, respectively. An adequate precision value of 19.23 further highlights the model's strong predictive performance.

3D surface plots (Figure 5) illustrate the interactions between variables affecting Pb^{2+} adsorption by ZnS-loaded biochar. Figure 5a shows that adsorption efficiency increases with pH and contact time, peaking at pH 6, but declines beyond this point due to reduced competition from hydronium ions at higher pH levels. Longer contact times enhance efficiency by allowing more ion-surface interactions. Figure 5b reveals that while pH 6 is optimal, efficiency decreases as initial Pb^{2+} concentration rises, due to saturation of active sites on the biochar. Figure 5c highlights that prolonged contact time improves adsorption, but higher initial concentrations reduce efficiency, again due to limited active site availability. These plots demonstrate how pH, contact time, and concentration influence adsorption efficiency.

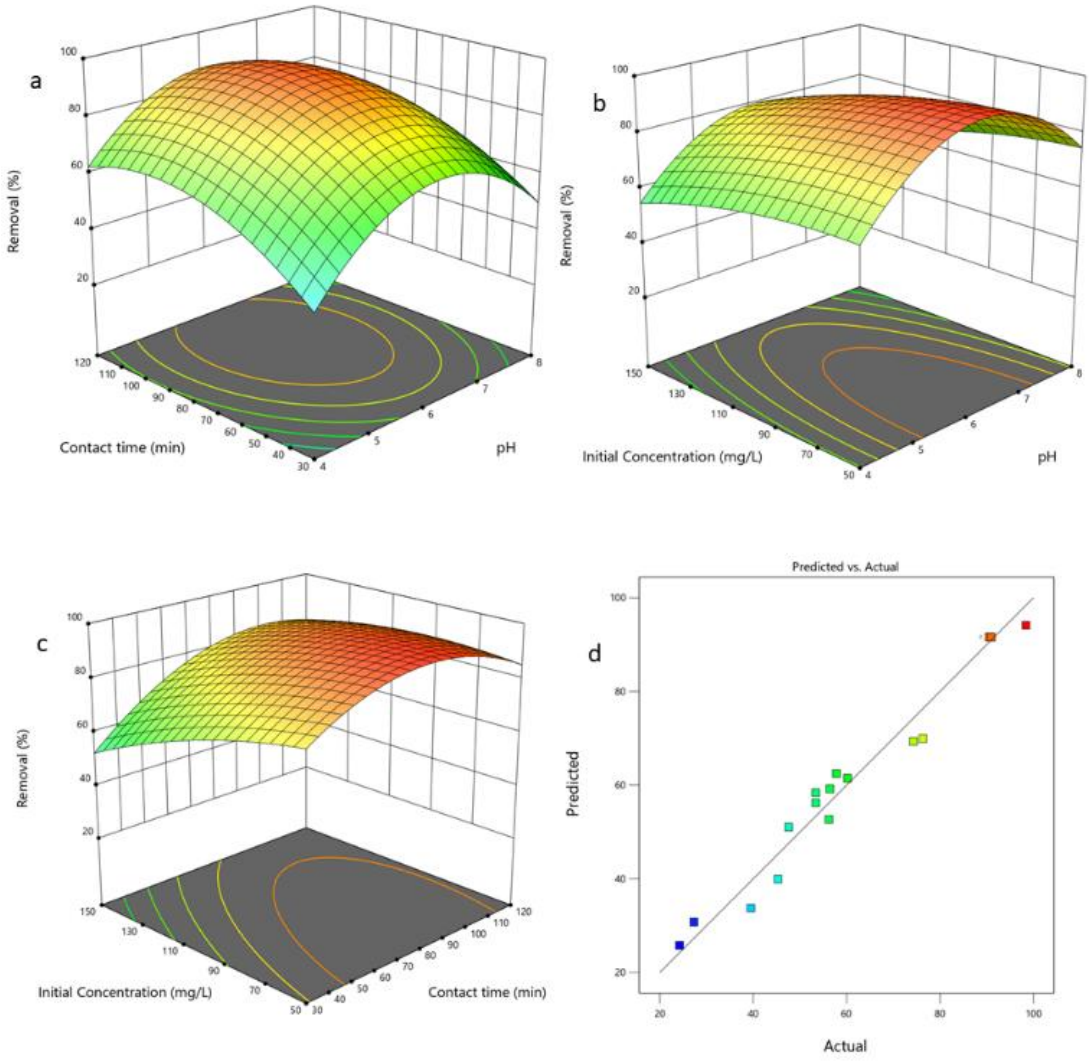

Figure 5. 3D surface plots of Pb^{2+} ions removal by ZnS loaded biochar a) pH vs Contact time

3.3 Adsorption isotherm

Mathematical models play a critical role in adsorption studies by providing insights into the adsorption process [15]. Isotherms, in particular, offer specific information about the binding interactions between the adsorbate and the adsorbent. For this study, three predominant isotherm models were applied to evaluate the equilibrium data for the adsorption of Pb^{2+} ions using metal nanoparticles. Table 3 summarizes the constants and correlation coefficients. The Freundlich isotherm yielded a moderate correlation coefficient (0.936), indicating a limited representation of the adsorption process. The Freundlich constant K_f value of 2.37 indicates a significant adsorption capacity, and the high adsorption intensity (n) value of 212.0 surpasses the model's interpretive range. Conversely, the Langmuir isotherm model exhibited a correlation coefficient of 0.999, signifying an excellent fit to the experimental data. The superior performance of the Langmuir model is further corroborated by the close alignment of its loading capacity values with both experimental and theoretical results [16]. These findings imply that the adsorption of Pb^{2+} ions onto ZnS-loaded biochar occurs as a uniform monolayer on the nanocomposite surface. To delve deeper into the adsorption mechanism, the Dubinin–Radushkevich (D-R) isotherm was also applied to the equilibrium data. The calculated mean potential energy (E_s) was 10.22 kJ/mol, suggesting that the Pb^{2+} ion adsorption by ZnS-loaded biochar proceeds primarily through ion exchange.

Table 3. Isotherm constants and correlation coefficients

Model	equation	Parameters	Values
Freundlich	$logq_{e=}logK_f + \frac{1}{n}logC_e$	K_f	2.37
		1/n	0.028
		R^2	0.936
Langmuir	$\frac{C_e}{q_e} = \frac{1}{bV_m} + \frac{C_e}{V_m}$	b	0.041
		V_m	212.0
		R^2	0.999
D-R	$lnq_e = lnq_m - \beta\varepsilon^2$ $\varepsilon = RTln(1 + \frac{1}{C_e})$ $E_s = \frac{1}{\sqrt{2K_D}}$	K_D	7×10^{-9}
		E_s	10.22
		R^2	0.892

3.4 Kinetic investigations

The reaction rate sheds light on the adsorption process of metal ions onto the adsorbent, and kinetic data obtained by varying time can be analyzed using models such as the Pseudo-First Order (PFO), Pseudo-Second Order (PSO), and intraparticle diffusion models [17]. The corresponding correlation coefficients are summarized in Table 4. The higher k_1 values indicate that ZnS-loaded biochar exhibits a rapid adsorption capacity for Pb^{2+} ions from aqueous solutions. The correlation coefficients for both PFO and PSO models were nearly equal to one, highlighting their strong ability to describe the adsorption process. However, when comparing theoretical and experimental loading capacities, PSO values showed better agreement. This suggests that the adsorption process is predominantly governed by electron transfer and chemisorption as the rate-limiting step [18]. Nevertheless, for chemisorption to be conclusively identified as the rate-limiting step, specific conditions outlined in existing studies must be met. A more detailed investigation is necessary to validate these conditions and confirm the adsorption mechanism.

Table 4. Kinetics constants of the ZnS loaded biochar for the removal of Pb^{2+} ions

Model	equation	Parameters	values
Pseudo first order	$\ln(q_e - q_t) = \ln q_e - k_1 t$	k_1	0.149
		q_e	39.2
		R^2	0.973
Pseudo second order	$\frac{t}{q_t} = \frac{1}{K_2 q_e^2} + \frac{t}{q_e}$	k_2	0.024
		q_e	107.2
		R^2	0.999

3.5 Thermodynamics of adsorption

To investigate the factors for the removal of Pb^{2+} ions by ZnS loaded biochar, the change in free energy (ΔG^0), enthalpy (ΔH^0), and entropy (ΔS^0) of the system were calculated using the following equations

$$\Delta G^\circ = -RT\,lnK_D \quad (4)$$

$$\Delta G^\circ = \Delta H^\circ - T\Delta S^\circ \quad (5)$$

$$lnK_D = \frac{\Delta S^\circ}{R} - \frac{\Delta H^\circ}{RT} \quad (6)$$

3.6 Where R is gas constant and T is temperature

The study uncovered intriguing insights into the change in free energy (ΔG°) during the adsorption process, as summarized in Table 5. Across all tested temperatures, ΔG° remained negative, indicating that the adsorption process was spontaneous. However, the magnitude of the negative values decreased with rising temperature, suggesting a reduction in spontaneity. This trend may be attributed to two factors: a weakening of the adsorption sites on the ZnS loaded biochar surface and an increase in the kinetic energy of Pb^{2+} ions in the solution. The negative enthalpy (ΔH°) confirmed the exothermic nature of the process, signifying that heat is released during adsorption. Additionally, the positive entropy (ΔS°) values suggest an increase in randomness, likely associated with the heat released during the adsorption process [19].

Table 5. Thermodynamic constants for the removal of Pb^{2+} ions by ZnS loaded biochar

Temperature (K)	Free energy ($\triangle G^0$)	Enthalpy ($\triangle H^0$)	Entropy ($\triangle S^0$)
303	-4304.9	-1392.1	589.9
313	-3971.2		
323	-3637.8		

3.7 Desorption and regeneration

Regenerating and reusing adsorbents is crucial for assessing their practical applicability in real-world scenarios. In this study, efforts were made to regenerate and reuse ZnS loaded biochar for the adsorption of Pb^{2+} ions from aqueous solutions. The results of these investigations are presented in Fig. 6a. Four desorbing agents HCl, CH_3COOH, NaOH, and Na_2CO_3 were evaluated for their effectiveness in regenerating ZnS loaded biochar. Among these, HCl demonstrated the highest efficiency due to its strong acid properties, which generate more hydronium ions compared to the organic acid and bases. Consequently, HCl was selected for further regeneration studies. The regenerated ZnS loaded biochar was reused over five cycles, with the removal efficiencies for each cycle illustrated in Fig. 6b. The removal efficiencies remained consistent during the first two cycles but declined in subsequent cycles. This decline is attributed to the repeated acid treatments, which weakened the adsorption sites. These findings indicate that ZnS loaded biochar can be effectively reused for up to two cycles without compromising its maximum removal efficiency.

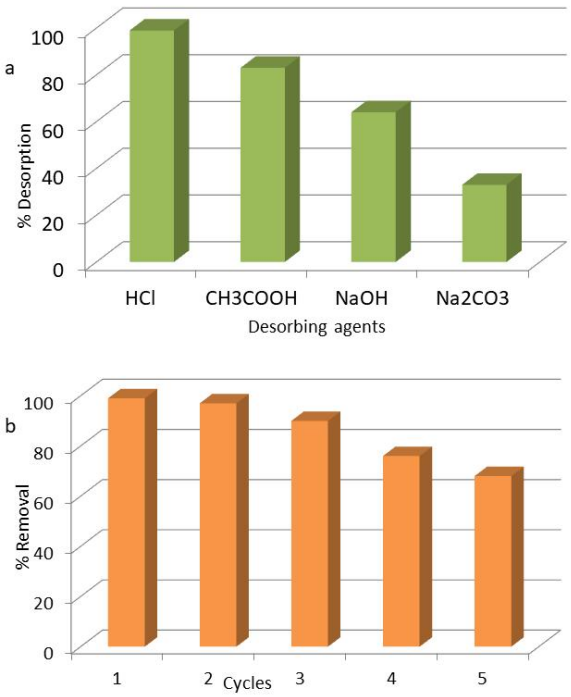

Figure 6. Desorption and regeneration plots for the removal of Pb^{2+} ions by ZnS loaded biochar

4 Mechanism of adsorption

Understanding the mechanism of adsorption of Pb^{2+} ion by ZnS loaded biochar is key to plan for real time applications. In this study the mechanism was determined to be ion-exchange based on the D-R isotherm, pH and regeneration investigations. The mean potential energy value (E_s) was found to be 10.22 which fall in the range of ion-exchange value and in addition to this at low pH the adsorption is found to be less due to competitive adsorption onto the surface by H^+ ions competing with Pb^{2+} ion. With increase in pH, the concentration of H^+ ions comes down and the rate of adsorption of Pb^{2+} ions increases suggesting the electrostatic attraction and ion exchange process. Further, the successful regeneration of the ZnS loaded biochar with HCl supports the ion-exchange mechanism involvement in the process.

5 Conclusion

This study synthesised the ZnS nanoparticles via green synthesis and the synthesis nanoparticles were loaded onto the biochar of jamun seeds. The prepared nanocomposite characterization revealed the successful loading of ZnS nanoparticles onto the biochar. The nanocomposite was applied in

adsorption of Pb^{2+} ions and the independent variables were optimised using CCD. The p-value and F-value highlighted the applicability of the model being significant. The adsorption capacity was calculated to be 212.0 mg g^{-1} which was high. The Langmuir isotherm and kinetic pseudo second order explained the equilibrium data. The thermodynamic values highlighted the spontaneity of the nanocomposite to adsorb Pb^{2+} ions. Desorption and regeneration studies suggested the merits of the nanocomposite in industrial applications. The mechanism of adsorption was determined to be ion-exchange for the removal of Pb^{2+} ions by ZnS loaded biochar. These results suggest that the ZnS loaded nanocomposite is a promising adsorbent for the removal of Pb^{2+} ions from aqueous solution.

Conflicts of interest

Authors declare no conflict of interest

Data statement

All the required data are available within the manuscript and any additional data are available with corresponding author on reasonable request

Contribution statement

VVD: Investigation, Manuscript writing, Validation; SR: Investigation, Manuscript writing, Characterization; PS: Formal analysis and characterization; ILRR: Validation, Review and editing of manuscript; RL: Conceptualization, Validation, Review and editing of manuscript;

References

[1] P. B. Tchounwou, C. G. Yedjou, A. K. Patlolla, and D. J. Sutton, "Heavy metal toxicity and the environment," in Molecular, Clinical and Environmental Toxicology, A. Luch, Ed. Basel: Springer, 2012, pp. 133–164.

[2] S. Ali et al., "Recent trends and sources of lead toxicity: A review of state-of-the-art nano-remediation strategies," J. Nanopart. Res., vol. 26, no. 168, 2024.

[3] A. Kumar et al., "Lead toxicity: Health hazards, influence on food chain, and sustainable remediation approaches," Int. J. Environ. Res. Public Health, vol. 17, no. 7, p. 2179, 2020.

[4] K. Harsha Vardhan, P. Senthil Kumar, and R. C. Panda, "A review on heavy metal pollution, toxicity, and remedial measures: Current trends and future perspectives," J. Mol. Liq., vol. 290, p. 111197, 2019.

[5] I. R. Chowdhury et al., "Removal of lead ions (Pb^{2+}) from water and wastewater: A review on the low-cost adsorbents," Appl. Water Sci., vol. 12, no. 8, pp. 185, 2022.

[6] N. Feng, X. Guo, and S. Liang, "Adsorption study of copper (II) by chemically modified orange peel," J. Hazard. Mater., vol. 164, no. 2–3, pp. 1286–1292, 2009.

[7] P. J. C. Isaac, R. Lakshmipathy, and A. Sivakumar, "Sunlight and microwave induced preparation of activated carbons and their removal of lead (II) and cadmium (II) from industrial effluent," Desalination Water Treat., vol. 53, no. 10, pp. 2701–2711, 2015.

[8] T. Iqbal et al., "Utilization of a newly developed nanomaterial based on loading of biochar with hematite for the removal of cadmium ions from aqueous media," Sustainability, vol. 13, no. 4, p. 2191, 2021.

[9] T. Saravanakumar et al., "Ultrasensitive humidity sensor based on flower-shaped α-MnO_2 nanostructures: Synthesis, characterization, and performance analysis," Mater. Sci. Semicond. Process., vol. 149, p. 106960, 2022.

[10] C. Wang and H. Wang, "Pb(II) sorption from aqueous solution by novel biochar loaded with nano-particles," Chemosphere, vol. 192, pp. 1–4, 2018.

[11] K. Zhang et al., "The role of biochar nanomaterials in the application for environmental remediation and pollution control," Chem. Eng. J., vol. 492, p. 152310, 2024.

[12] R. Lakshmipathy et al., "ZnS nanoparticles capped with watermelon rind extract and their potential application in dye degradation," Res. Chem. Intermed., vol. 43, pp. 1329–1339, 2017.

[13] D. Martínez, M. Motevalli, and M. Watkinson, "Is there really a diagnostically useful relationship between the carbon–oxygen stretching frequencies in metal carboxylate complexes and their coordination mode?" Dalton Trans., vol. 39, no. 2, pp. 296–310, 2010.

[14] S. Wei and Q. Zheng, "Biosynthesis and characterization of zinc sulphide nanoparticles produced by the bacterium Lysinibacillus sp. SH74," Ceram. Int., vol. 50, no. 2, Part A, pp. 2637–2642, 2024.

[15] H. Hinsene, N. Bhawawet, and A. Imyim, "Rice husk biochar doped with deep eutectic solvent and Fe_3O_4/ZnO nanoparticles for heavy metal and diclofenac removal from water," Sep. Purif. Technol., vol. 339, p. 126638, 2024.

[16] S. Ali et al., "Chitosan-supported ZnO nanoparticles: Their green synthesis, characterization, and application for the removal of pyridoxine HCl (Vitamin B6) from aqueous media," Molecules, vol. 29, no. 4, p. 828, 2024.

[17] R. S. Sodhi et al., "Biogenic synthesis of ZnO nanoparticles using Polystichum squarrosum extract and its applications as antioxidant, antidiabetic agent, and in industrial wastewater treatment," Emergent Mater., vol. 7, no. 2, pp. 285–298, 2024.

[18] R. Zhao, H. Gao, L. Duan, and R. Yu, “Synergistic toxic effects of high-strength ammonia and ZnO nanoparticles on biological nitrogen removal systems and role of exogenous C10-HSL regulation,” J. Environ. Sci., vol. 150, pp. 385–394, 2025.

[19] S. Hussain et al., “Fabrication of carboxymethyl cellulose/graphene oxide/ZnO composite hydrogel for efficient removal of fuchsin dye from aqueous media,” Int. J. Biol. Macromol., vol. 277, no. 1, p. 134104, 2024.